Cite this article
El Mahboub E, Zakaria S, El Hichou A and Mansori M (2025)
Impact of heating on the properties of CZTS thin film solar cells produced through sol-gel spin-coated.
Nanomaterials and Energy **14(4)**: 170–182,
https://doi.org/10.1680/jnaen.24.00066

Research Article
Paper 2400066
Received 19/04/2024; Accepted 18/07/2025

Nanomaterials and Energy

Impact of heating on the properties of CZTS thin film solar cells produced through sol-gel spin-coated

Elyazid El Mahboub
IMED-Lab.: Groupe d'Étude des Matériaux Optoélectroniques (GEMO), Faculty of Science and Technology, Cadi Ayyad University, Marrakech, Morocco

Sanaa Zakaria
IMED-Lab.: Groupe d'Étude des Matériaux Optoélectroniques (GEMO), Faculty of Science and Technology, Cadi Ayyad University, Marrakech, Morocco

Ahmed El Hichou
IMED-Lab.: Groupe d'Étude des Matériaux Optoélectroniques (GEMO), Faculty of Science and Technology, Cadi Ayyad University, Marrakech, Morocco (corresponding author: a.elhichou@uca.ma)

Mohammed Mansori
IMED-Lab.: LCME, Laboratoire de Chimie des Matériaux et d'Environnement, Faculty of Science and Technology, Cadi Ayyad University, Marrakech, Morocco

This paper investigates the influence of annealing temperatures on the properties of copper-zinc-tin sulfide (CZTS) thin films synthesized using a low-cost sol-gel spin-coating technique. The thin films were annealed at different temperatures: 340°C, 360°C, 380°C, and 400°C. Analysis of the X-ray diffraction data revealed a consistent kesterite structure in all thin films, with a preferred orientation along the (112) plane. Raman's spectra confirmed the purity of the phase and confirmed the presence of the CZTS kesterite structure. The morphological and elemental compositions of the thin films showed significant fluctuations in response to changes in annealing temperature. This effect is due to the influence of temperature on the reaction dynamics during the preparation of the deposition solution. The optical properties showed a robust absorption coefficient (>10^4 cm^{-1}) with optical bandgaps ranging from 1.38 to 1.72 eV. In particular, the CZTS sample annealed at 340°C showed superior crystallinity and outperformed others in optical and electrical properties. To expand the practical implications, the parameters derived from this study were theoretically integrated into a solar cell model (CZTS/(CdS or ZnS)/ZnO:i). Using SCAPS-1D simulation, efficiencies of 11.40% and 10.55% were predicted for the CdS and ZnS buffer layers, respectively. These results provide valuable information for optimizing CZTS thin films to improve solar cell performance.

Keywords: annealing/CZTS thin films/SCAPS-1D/semi-conductors/solar cells/sol-gel/thin films

1. Introduction

Copper-zinc-tin-sulfide kesterite compounds (Cu_2ZnSnS_4 or CZTS) have attracted considerable attention in recent years due to their desirable optoelectronics properties for photovoltaic (PV) thin film solar cell applications.[1] It is a promising material for solar cells because it is an abundant, low-cost, and environmentally friendly material that offers significant advantages over CIGS and CdTe.[2] Both CdTe and CIGS have significant disadvantages, such as the toxicity of Cd, scarce resources of the elements In, Ga, and Te, and resulting price fluctuations that could affect their market launch in the future. Furthermore, the same underlying device architecture for CdTe and CIGS could be implemented for CZTS, which would help accelerate the development of CZTS solar cells with superior power conversion efficiencies.

CZTS has a remarkably high absorption coefficient in the visible region, which is 104 cm^{-1}.[3] Its optimal forward bandgap of 1.5 eV strategically positions it to efficiently capture a significant portion of the visible solar spectrum.[4] CZTS is characterized by its p-type conductivity and is the ideal choice among second-generation thin film solar cells.

The theoretical limit of energy efficiency of CZTS connections is an impressive 32%.[5] It is noteworthy that a breakthrough was achieved in 2012 with a record CZTS conversion efficiency of 12.6%, using a pure hydrazine-based solution route.[6] Various techniques have been used to prepare CZTS thin films, including molecular beam epitaxy,[7] sputtering,[8] pulsed laser deposition,[9] sputter pyrolysis,[10] electrodeposition,[11] and sol-gel spin-coating. Among these methods, the sol-gel process stands out for its simplicity, which allows it to be adapted to large surfaces and different substrates in terms of shapes and materials. In addition, the sol-gel technique offers advantages such as precise stoichiometric control and quantitative doping at the molecular level. This allows greater control over structure and composition compared to alternative methods. In this study, the sol-gel route was the main method for preparing CZTS films.

The performance of a solar cell depends mainly on the crystalline structure and the composition of the absorbing material. Therefore, it is important to understand and optimize the growth of photovoltaic materials to achieve the desired stoichiometry.[12] In fact, the stoichiometry of CZTS is influenced by the annealing temperature and the atmosphere.[13–15] It was found that good crystallinity requires higher growth temperatures. However, to avoid the evaporation of sulfur S during deposition, it is necessary to proceed with low temperature deposition and subsequent post-treatment at higher temperature to improve crystallinity. The sulfurization process ensures the best stoichiometry of the CZTS thin film, and the high temperature heating ensures the high crystallinity of the CZTS absorbing material, which improves the electrical and optical properties.[16] Xiaomi You *et al*.[17] studied the annealing of sol-gel based CZTS films prepared from sulfur-containing solutions in an inert atmosphere without suffixation and with different thicknesses of the deposited layers: three-layer samples annealed at 250°C for 10 min, five- and nine-layer samples were annealed at 500°C in a nitrogen atmosphere for 60 min. They showed that the CZTS phase was successfully formed in all samples, and the nine-layer sample had better crystallinity. In another study, Khottummee *et al*.[18] studied the influence of annealing temperature on the optical properties of CZTS thin films deposited by the dip coating technique using the sol-gel method. They showed that the bandgap energy decreases from 1.72 to 1.50 eV when the annealing temperature increases from 200°C to 500°C for 1 h. In addition, many studies have been conducted on the influence of annealing temperature,[19] temperature, and time[20,21] on CZTS thin films prepared by sol-gel spin coating.

In this study, we investigated the effect of annealing in air at different temperatures on the structural, morphological, elemental composition, optical and electrical properties of CZTS thin films synthesized by sol-gel spin-coating technique. The aim of this study was to determine the optimal annealing conditions. In addition, using the CZTS data from this research, the theoretical performance of the solar cell with a toxic buffer layer (CdS) and a non-toxic buffer layer (ZnS) was also determined using a solar cell capacitance simulator (SCAPS-1D).

2. Experimental procedures

2.1 Preparation of copper zinc tin sulfide

CZTS thin films were synthetized by sol-gel spin-coating technique on soda-lime glass using copper chloride ($CuCl_2.2H_2O$), zinc chloride ($ZnCl_2$), tin chloride ($SnCl_2.2H_2O$), and thiourea ($SC(NH_2)_2$) as precursors for copper (Cu), zinc (Zn), tin (Sn), and sulfur (S). The ratio of Cu:Zn:Sn:S was maintained at 2:1:1:8. The solution was stirred at 60°C for 20 min, then spin-coated onto cleaned glass substrates at 3000 rpm for 20 s and dried at 280°C for 10 min. This process was repeated to achieve the desired film thickness. The coated substrates were annealed in air at 340°C, 360°C, 380°C, and 400°C for 20 min, except for one sample left non-annealed to assess the impact. The samples were labeled as CZTS-AD, CZTS-340, CZTS-360, CZTS-380, and CZTS-400 accordingly.

2.2 Characterization technique

The film's crystalline structure was confirmed using X-ray diffraction (XRD) in a Bragg–Brentano geometry with CuKα radiation (λ = 1.5418 Å). Raman spectroscopy analyzed the phase composition of CZTS samples with a laser wavelength (λ = 532 nm) ranging from 200 to 500 cm^{-1}. Field-emission scanning electron microscopy (FESEM) and energy-dispersive X-ray spectrometry (EDX) were used to examine surface morphology and elemental composition of the thin films. FESEM images were taken with a fixed electron beam at 10 kV.

Optical studies were performed using a computer-controlled UV–vis–NIR spectrophotometer (UV-3101PC-SHIMADZU) covering a range of 185–1400 nm. Transmittance measurements were compared to bare glass substrates. Electrical properties were assessed by measuring the resistivity of the samples at room temperature using the van der Pauw method with an Ecopia HMS-5500 instrument.

2.3 Simulation detail

SCAPS is a one-dimensional solar cell simulation software developed by researchers at the Department of Electronics and Information Systems (ELIS) at Ghent University in Belgium.[22] We used SCAPS-1D to perform a numerical simulation of a CZTS solar cell, and determine its theoretical efficiency and key output parameters such as *J*–*V* characteristics.

3. Results and discussion

3.1 Structural properties

XRD was used to analyze the structural properties that influence the optical and electrical properties of CZTS thin films. Figure 1 shows the X-ray patterns of CZTS-AD, CZTS-340, CZTS-360, CZTS-380, and CZTS-400°C. The sample annealed at 400°C initially shows no CZTS peaks and is therefore unsuitable for optical and electrical evaluations. However, the remaining samples show sharp peaks at 28.34°, 47.38°, and 56.43°, denoted as (112), (220), and (312), respectively, indicating the thin film structure of CZTS. The XRD patterns confirm that all thin films crystallized in the kesterite structure (ICDD #04-023-3974). This is consistent with

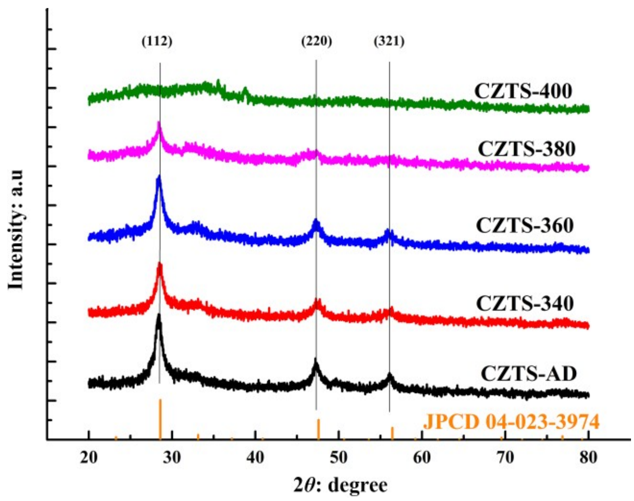

Figure 1. X-ray diffraction results of all CZTS thin films annealed at different temperatures

previous research,[13] which suggested that CZTS thin films should be annealed at the lowest possible temperature without sulfurization to avoid CZTS phase degradation and sulfur evaporation. Note that the peak (112) at 28.34° shows significant intensity in all samples, indicating the preferential orientation of the CZTS film along the (112) axis. The crystallinity of the films improves with increasing temperature up to 360°C, highlighting the tendency for CZTS crystalline structure to align along the (112) direction and confirming the formation of the CZTS kesterite crystallographic phase.

The crystal size D was calculated by exploiting the XRD results using the Debye–Scherrer relation:[23]

1. $$D = \frac{0.9\lambda}{\beta\cos(\theta)}$$

where β is full width at half maximum (FHWM), λ is the wavelength of the Cu(kα) radiation, and θ is the angle of the (112) peak. The crystalline size *D* versus annealing temperature is shown in Figure 2.

The CZTS-AD exhibits a minimum crystalline size of ≈8.72 nm. It is obvious that the crystalline size *D* with increasing annealing temperature and reaches 17.79 nm. This behavior suggests that higher annealing temperatures result in larger crystalline sizes, possibly due to the increased thermal energy of the atoms.[24] It is well documented that the conversion efficiency of CZTS solar cells improves with larger grain sizes in the absorber layer. However, these average crystalline sizes are smaller than those achieved with CZTS thin films annealed through sulfurization.[25] Therefore, annealing in air at temperatures exceeding 380°C could potentially affect the crystallinity and phase purity, leading to the formation of secondary impurity phases.

3.2 Raman spectroscopy

Raman spectroscopy was used to definitively identify the CZTS kesterite phase. The similarity between the XRD databases for cubic ZnS and tetragonal Cu_3SnS_4 and CZTS makes it difficult to distinguish CZTS based on XRD results alone. An Ar^+ laser with a wavelength of 532 nm was used for the analysis. In Figure 3, the Raman spectra of pre-annealed and annealed CZTS thin films at different temperatures are shown. The Raman data revealed a consistent peak at 337 cm^{-1} in all CZTS thin films, which corresponds to the main vibration mode A1characteristic of the CZTS phase.[26] Consequently, both Raman spectra and XRD data confirmed the formation of a pure kesterite crystallographic phase in the CZTS thin films.

3.3 Surface morphological and its composition

The CZTS thin films were analyzed using SEM images to investigate the influence of annealing and non-annealing temperatures on their surface morphology. SEM images are shown in Figure 4. A significant difference in morphology was observed between the pre-annealed and annealed samples. The images reveal numerous nanopores on the surface of all thin films, probably due to evaporation of precursors during the drying process, especially for thiourea precursors. Park *et al*.[27] demonstrated through thermalgravimetric analysis that thiourea exhibited the highest weight loss compared to other precursors at 250°C. Despite drying the samples at 280°C, all samples showed particle agglomeration, non-uniform surfaces, and cracks of different sizes. Nanocavities were also present. Increasing the annealing temperature resulted in a smoother surface. The SEM image of the sample annealed at 380°C shows a dense and almost uniform surface morphology with small cracks and voids (Figure 4(d)).

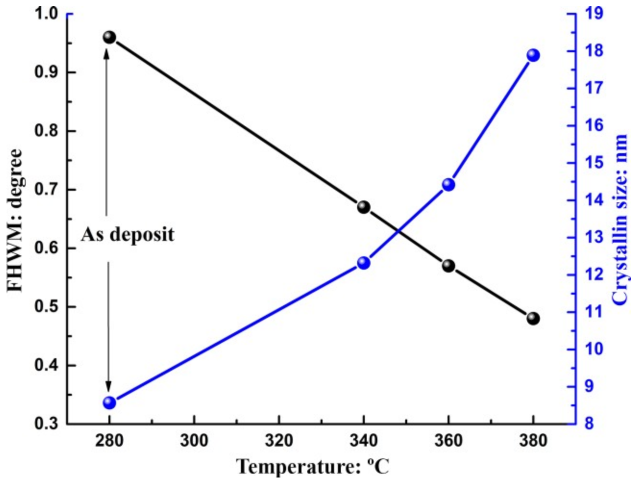

Figure 2. Crystalline size and FHWM plotted against the annealing temperatures

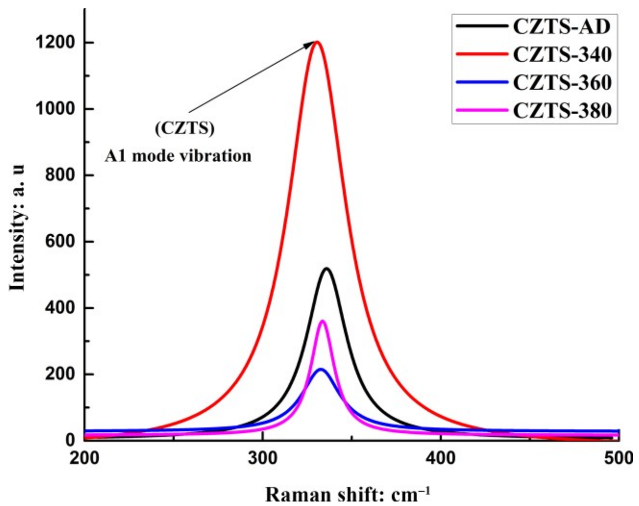

Figure 3. Raman spectroscopy results of all CZTS thin film

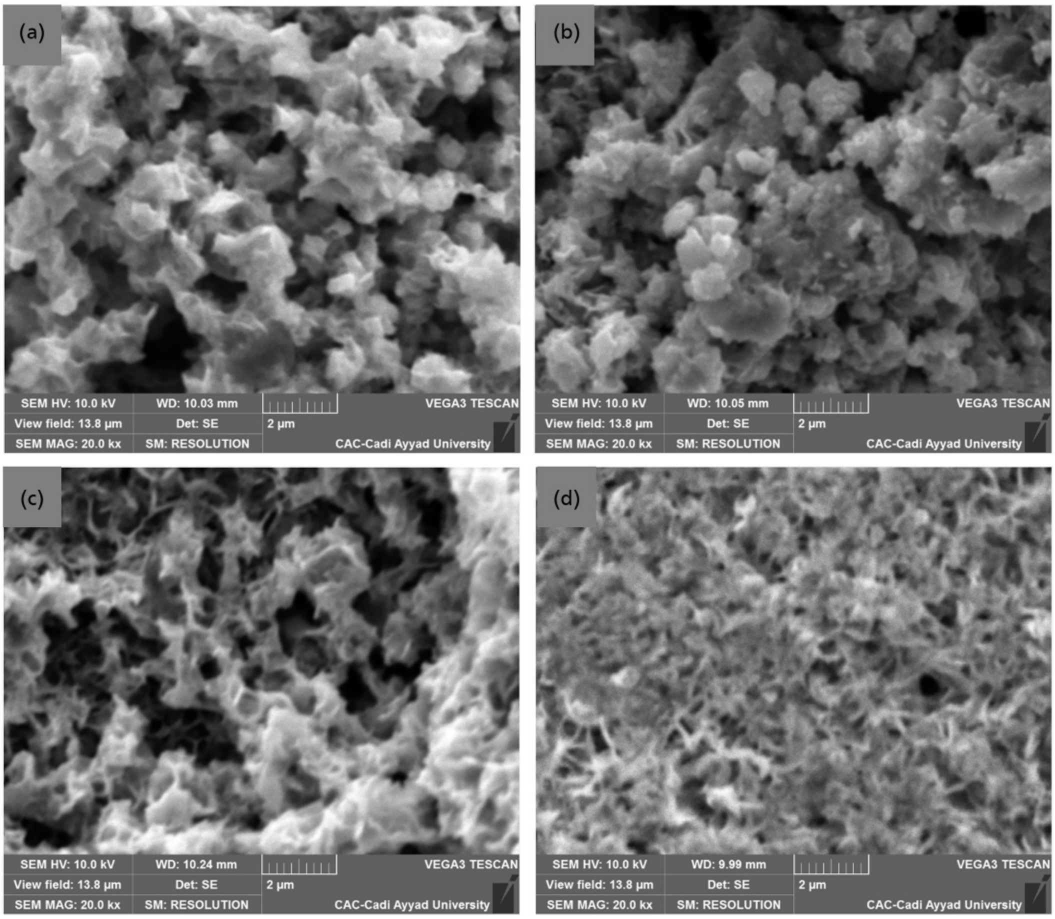

Figure 4. Surface morphological of CZTS-AD (a), CZTS-340 (b), CZTS-360 (c), and CZTS-380 (d)

The elemental composition of CZTS significantly influences its crystal structure and its efficiency in solar cells.[28] Heat treatment is a crucial factor in determining the initial composition of CZTS in a solution. A higher efficiency was observed for non-stoichiometric Cu-poor, Zn-rich.[29] EDX coupled with SEM was utilized to analyze the composition of CZTS thin films, detecting variable atomic percentages of Cu, Zn, Sn, and S at different annealing temperatures (Figure 5 and Table 1). The CZTS-340 and CZTS-360 exhibited Cu-poor and Zn-rich configurations which are suitable for the growth of high-quality CZTS thin films. However, the element ratios Cu/Zn + Sn and Zn/Sn of the annealed CZTS thin films slightly increased, while the S/metal ratio decreased with increasing annealing temperature (Figure 6). XRD and EDX analysis demonstrated that the high crystallinity was observed for the Cu-poor Zn-rich represented by CZTS-340 (Cu/Zn + Sn = 0.67, Zn/Sn = 1.05), and also for the CZTS-360 (Cu/Zn + Sn = 0.95, Zn/Sn = 1.14). Thus, these conditions could be developed for growing high-crystallinity CZTS thin films and yielded highest conversion efficiency.

Additional elements such as O, C, and Cl were identified in the analysis. The presence of carbon could be due to the incomplete evaporation of the solvent and thiourea, while the presence of chloride could be due to the metal chloride used. The atomic content of carbon significantly influences the electrical properties of CZTS thin films. The inclusion of metal chloride is intended to reduce the carbon content, which decreases with increasing temperature rises and reaches a minimum at 360°C.

3.4 Optical properties

The optical properties of CZTS thin films annealed at different temperatures were analyzed by UV–visible spectroscopy in the wavelength range of 360–1100 nm. Figures 7 and 8 present the optical transmission spectra (T) and reflection spectra (R) spectra of the CZTS thin films, respectively. Consistent changes in transmittance and reflectance were observed at all wavelengths except for CZTS-AD, which remained constant. The CZTS sample annealed at 360°C exhibited the highest transmittance and reflectance, which may be due to the surface morphology and elemental composition.

The transmission and reflectance results were used to calculate the optical bandgaps for all CZTS thin films, based on the Tauc method using the following relation:[30]

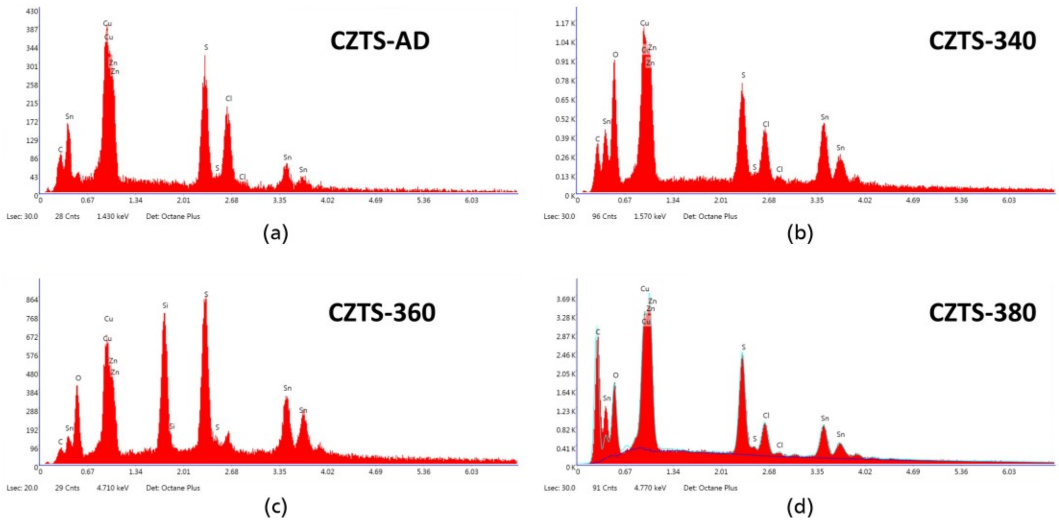

Figure 5. EDX spectrum of CZTS-AD (a), CZTS-340 (b), CZTS-360 (c) and CZTS-380 (d)

Table 1. The compositional of all CZTS thin films and the elements ratio Zn/Sn, Cu/Zn + Sn, and S/metal

Element	CZTS-AD	CZTS-340	CZTS-360	CZTS-380
Cu (at%)	10.53	11.07	16.71	13.47
Zn (at%)	8.49	8.18	9.39	7.69
Sn (at%)	4.58	4.27	8.18	2.65
S (at%)	18.21	17.65	18.91	6.98
C (at%)	45.45	46.21	20.43	50.82
O (at%)	—	—	26.37	16.75
Cl (at%)	12.73	12.63	—	1.63
Zn/Sn	1.85	1.05	1.14	3.41
Cu/Zn + Sn	0.80	0.67	0.95	1.65
S/Cu + Zn + Sn	0.78	0.75	0.35	0.29

2. $$\alpha \mathrm{hv} = B.(\mathrm{hv} - \mathrm{E_g})^{\frac{1}{2}}$$

where E_g is the bandgap, B is a constant independent of the energy hv, and α is the absorption coefficient determined for all samples using the following formula:

3. $$\alpha = \frac{1}{\mathrm{d}} \ln\left(\frac{(\mathrm{R} - \mathrm{T})^2}{\mathrm{T}}\right)$$

where d is the thickness of the thin film estimated to be 3 µm from the SEM image from our previous work.[31] All CZTS thin films show an absorption coefficient of $10^4\,\mathrm{cm}^{-1}$ in the visible region which is consistent with previous results reported in other works,[15,32] and are suitable for use as absorption layers in thin-film solar cells.

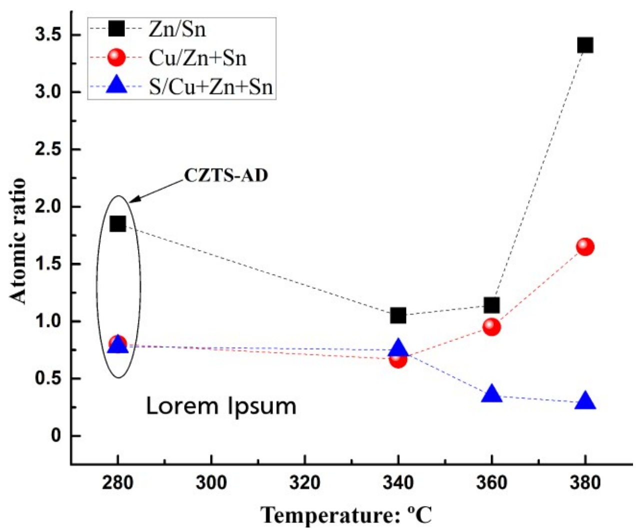

Figure 6. The ratio Zn/Sn, Cu/Zn + Sn, and S/metal variation with the annealing temperature

The optical bandgap indicates the range of the solar spectrum that a photovoltaic cell can absorb. The bandgap energy was calculated by extrapolating the linear portion of $(\alpha hv)^2$ versus the incident photon energy hv, as shown in Figure 9. The bandgap values range from 1.38 to 1.71 eV with increasing annealing temperatures, while CZTS-AD exhibits a minimum bandgap of 1.36 eV. The increase in bandgap with increasing the annealing temperatures is attributed to variations in crystalline quality and resulting differences in grain sizes among the samples. In our study, the decrease in S/metal ratio with increasing annealing temperature is associated with an increase in bandgap energy. Previous studies on CZTS synthesized using sputtering and thermal evaporation methods

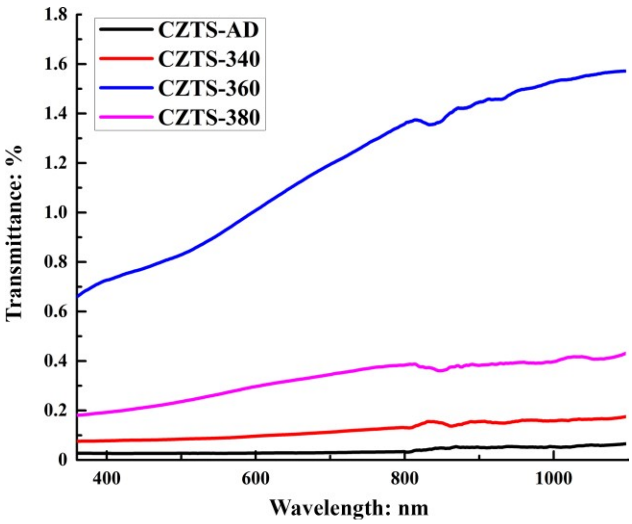

Figure 7. Transmittance spectra plotted against wavelength

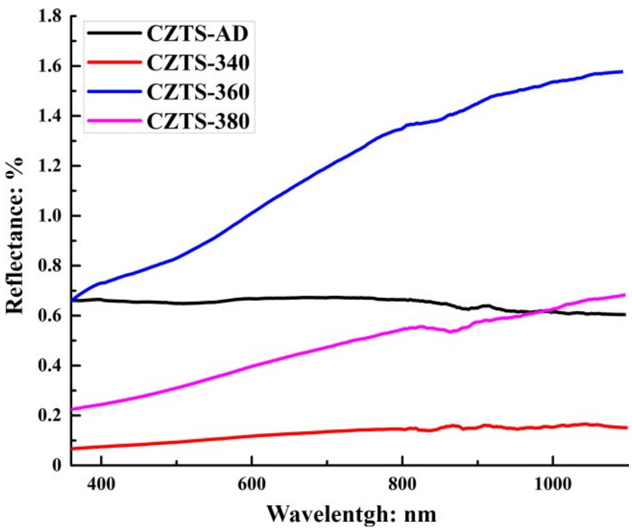

Figure 8. Reflectance spectra plotted against wavelength

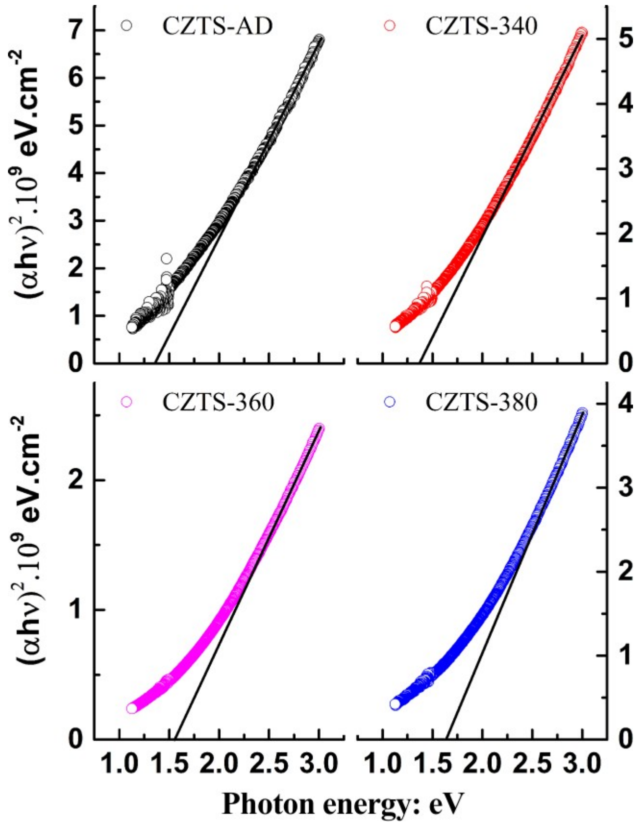

Figure 9. Optical bandgap of all CZTS thin films determined by Tauc method

have shown that the bandgaps of CZTS thin films increase with annealing temperature, which agrees well with our results.[33,34] The optical bandgaps of all obtained CZTS samples are considered suitable for the use of solar cells.[35]

3.5 Electrical properties

The electrical properties of CZTS have a significant impact on the efficiency of solar cells. To analyze the electrical properties of CZTS thin films deposited and annealed at different temperatures, the four-point method was used. Table 2 describes the resistivity, conductivity type, and hole concentration determined from Hall effect measurements. All CZTS thin films exhibited p-type conductivity. The resistivity of the annealed CZTS samples varies with temperature and is directly influenced by the film properties and crystallinity. This change is related to the increase in bandgaps and composition of CZTS with annealing temperatures. A larger crystallite size reduces grain boundaries, minimizing film defects and carrier recombination.[36] The CZTS-360 sample showed minimal resistivity (1.60×10^{-2} Ωcm) due to the low carbon content and Cu/Zn + Sn ratio observed in the EDX results. The lack of Cu led to the formation of the CuZn antisite defects, which are the main reason for the p-type conductivity and good electrical properties of the CZTS thin film.[37] The resistivity values of all CZTS thin films were consistent with the literature.[38] However, as the S/metal ratio in annealed CZTS decreased, the mobility and hole concentration also decreased. Petal *et al*. have shown that high mobility is related to Zn-rich and high S content.[39] Other study revealed that the electrical properties of CZTS are influenced by the stoichiometry and atomic percentage of each element.[40] All electrical parameters of the sol-gel deposited CZTS absorption layer are suitable for photovoltaic applications.

4. *I*(*V*) characteristics

In this study section, CZTS thin films with p-type conductivity were deposited on an ITO substrate with n-type conductivity to create a PN junction, which was confirmed by their electrical

Table 2. Electrical results of CZTS thin films

Samples	Type	Resistivity: Ω cm	Mobility: cm^2/Vs	Hole concentration: cm^{-3}
CZTS-AD	p	1.84×10^{-2}	18.51	5.821×10^{17}
CZTS-340	p	4.05×10^{-2}	24.66	1.665×10^{16}
CZTS-360	p	1.60×10^{-2}	14.67	1.228×10^{16}
CZTS-380	p	9.98×10^{-2}	9.78	1.916×10^{15}

properties. An Ag contact was then placed on top of the CZTS to improve current flow. Figure 10 shows the *I–V* properties of CZTS thin films deposited on an ITO substrate using sol-gel spin-coating in the absence of light. The semi-logarithm of *I*(*V*) is shown in the inset of Figure 10. The nonlinear *I–V* characteristics demonstrate rectifying and non-ohmic behavior, indicating the successful formation of a PN junction between the p-CZTS and n-ITO thin films. Furthermore, the *I–V* curve showed a turn-on voltage of 0.45 V. In addition, the positive part of the *I–V* curve, which shows an exponential variation, can be modelled using the following equation:

4. $$I(V) = I_0\left(e^{\frac{qV}{nkT}} - 1\right)$$

where I_0 is the saturation current estimated at 3.1×10^{-5} A, q is the electronic charge, V is the voltage applied to the terminals of the junction, k is the Boltzmann constant, T is the temperature in Kelvin, and n is the ideality factor which is an important parameter. However, each diode has an ideality factor. For solar cell applications, the ideality factor n is in the range of 1–2.

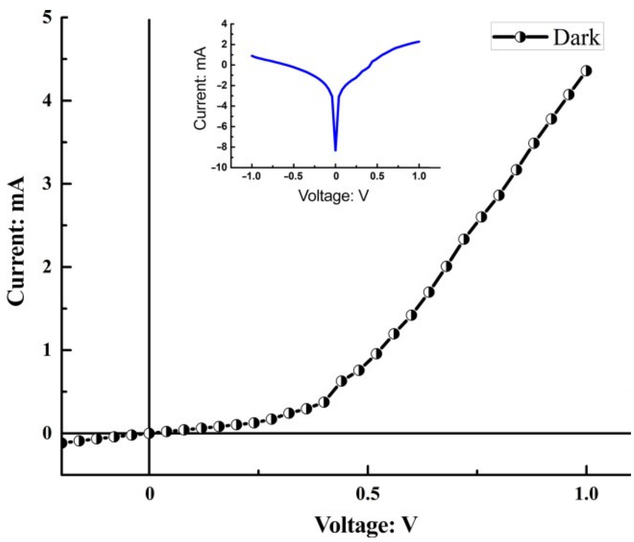

Figure 10. *I–V* characteristic of CZTS thin films deposited with sol-gel spin-coating on ITO substrate

For the diode consisting of a heterojunction (glass/n-ITO/p-CZTS/Ag), the series resistance R_s must be taken into account due to the lattice mismatch between CZTS and ITO. This resistance is influenced by the contact resistances on the front and back. The series resistance was calculated to be 139.5 Ω based on the *I–V* curve analysis.

The PN junction structures (glass/n-ITO/p-CZTS/Ag) are shown in Figure 11, both in the dark and under illumination. The device showed consistent behavior under both conditions, with rectifying properties observed at the PN junction. In particular, the turn-on voltage dropped to 0.42 V and the measured ideality factor was 1.77 under lighting. Furthermore, an increase in current was observed during illumination, which is due to the photocurrent generated by the CZTS absorbing the incident photons. This process excites electrons from the valence band to the conductive band and forms electron–hole pairs,[41] resulting in improved PN junction parameters. The fabricated device can be used as a UV detector[36] and for photocatalytic applications.[42] The solar cell can use an our PN junction to incorporate a buffer layer between p-CZTS and n-FTO, reducing potential barriers due to lattice parameter mismatch. Gunavathy *et al.*[43] studied the influence of FTO substrate temperature on CZTS thin films prepared by spray pyrolysis. The sample annealed at 350°C showed promising properties and was

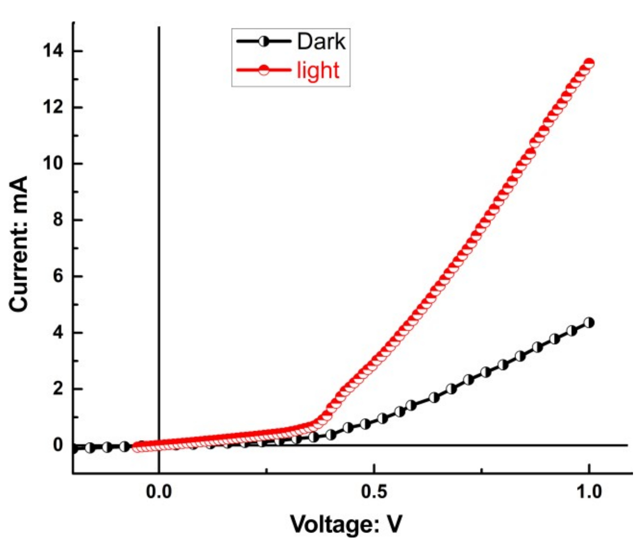

Figure 11. *I–V* characteristic in the dark and illumination of CZTS thin films deposited with sol-gel spin-coating on IFO substrate

used as a n-type in a heterojunction with the FTO/CdS/CZTS/Ag configuration. The PN junction showed rectifying behavior. However, under illumination, the solar cell characteristics for this heterojunction structure were: open-circuit voltage of 213 mV, short-circuit current density of 490 μA cm^{-2}, fill factor of 0.33%, and an efficiency of 0.68%.

5. Simulation part

This section explores the impact of non-annealing and annealing at different CZTS temperatures on solar cell efficiency using the SCAPS-1D capacitance simulator. SCAPS-1D can determine key parameters of solar cells such as: efficiency (η), fill factor (FF), short-circuit current density (J_{sc}), and open-circuit voltage (V_{oc}). Figure 12(a) shows the physical device used in this study, which is composed of Mo/CZTS/(CdS or ZnS)/ZnO:I layer. The simulated band energies of the devices with CdS and ZnS buffer layers are shown in subfigures (b) and (c) of Figure 12. In this configuration, Mo serves as the back contact, CZTS as the absorber layer, ZnO:I as the window layer, and ZnS and CdS as different buffer layers. For the buffer layer, a comparative study was performed between ZnS, which is abundant and non-toxic, and CdS to reveal the performant layer.[44] However, the scarcity and toxicity of cadmiums limits the cost efficiency of this buffer layer. Therefore, it is imperative to explore alternative materials to replace CdS. ZnS thin films offer several advantages over CdS as a buffer layer in solar cells.[45,46] The parameters for the SCAPS-1D simulation of all layers of the solar cell are detailed in Table 3 and are taken from the literature, except for CZTS-AD, CZTS-340, CZTS-360, and CZTS-380 (Table 4). Based on the results of this study, key parameters of these absorber layers were incorporated into SCAPS-1D. During the entire simulation under AM 1.5 illumination, the physical constants remained constant at a temperature of 300 K. Figures 13 and 14 show the current–voltage results for CZTS-AD and all annealed CZTS layers at different temperatures using CdS and ZnS as buffer layers, respectively. The parameters used for the SCAPS-1D simulation for all the layers in a solar cell are listed in Table 3 which are taken from the literature, except for those of CZTS-AD, CZTS-340, CZTS-360, and CZTS-380 (Table 4). Based on the results of this study, key parameters of the absorbent layers were integrated into SCAPS-1D. Throughout the simulation under AM 1.5 illumination, these physical constants were kept constant with the temperature set at 300 K. Figures 13 and 14 show the current–voltage results for CZTS-AD and all CZTS annealed at different temperatures using CdS and ZnS as buffers layers respectively. All SCAPS-1D results can be found in Table 5. Changes in the properties of CZTS have a significant impact on the parameters of solar cells. The modification of processes or annealing temperatures influences CZTS properties, subsequently affecting solar cell performance when CdS or ZnS is used as a buffer layer. The J_{sc} values of CdS and ZnS decrease

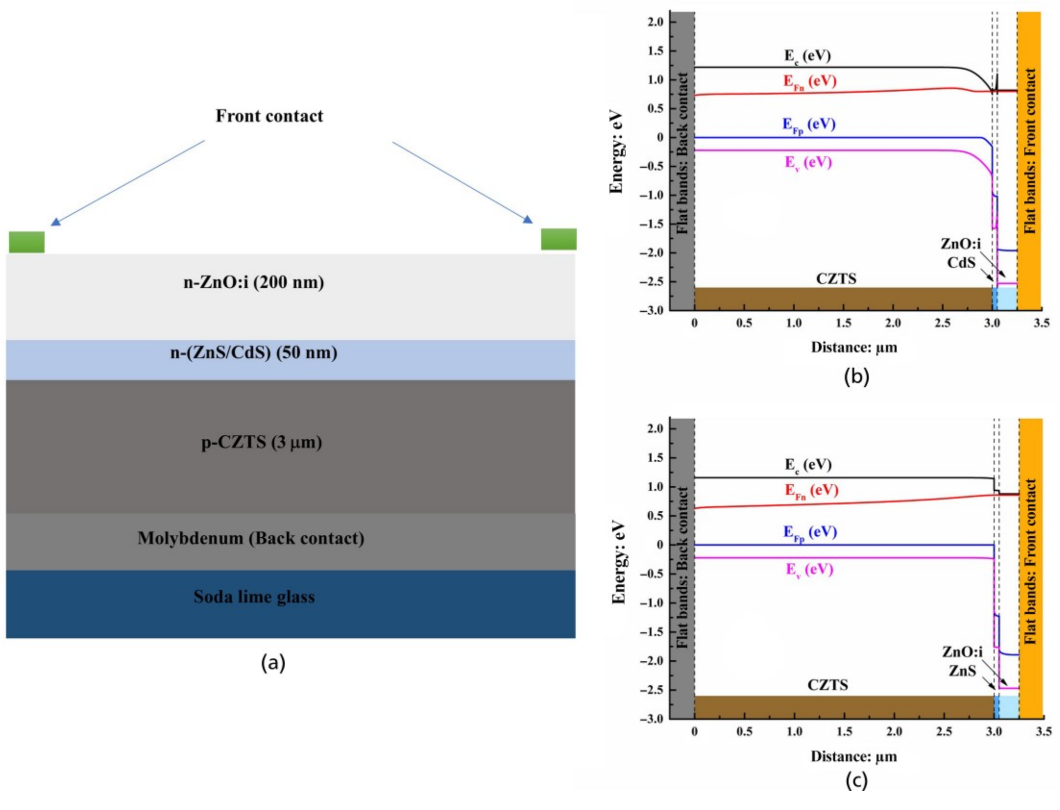

Figure 12. Solar cell structure using CZTS film (a) and simulated band energies of the devices with CdS (b) and ZnS (c) buffer layers

Table 3. The physical parameters of window layer (ZnO:i) and buffer layers (CdS and Zn(S.O))

Parameter	ZnO:I[55]	CdS[55]	Zn(S,O)[56]
Thickness: μm	0.200	0.050	0.050
Bandgap: eV	3.350	2.400	2.700
Electron affinity χ: eV	4.350	4.000	4.300
Dielectric permittivity	9.000	10.000	10.000
CB effective density of states: 1/cm^3	2.200×10^{18}	2.200E + 18	2.200E + 18
VB effective density of states: 1/cm^3	1.800×10^{19}	1.800E + 19	1.800E + 19
Electron mobility: cm^2/Vs	2.500×10^1	2.500×10^1	1.000×10^2
Hole mobility: cm^2/Vs	1.000×10^2	1.000×10^2	2.500×10^1
Shallow uniform donor density ND: cm^{-3}	1.000×10^{18}	1.000×10^{18}	1.000×10^{17}
Shallow uniform acceptor density NA: cm^{-3}	0.000×10^0	0.000×10^0	0.000×10^0

Table 4. Absorbents layer's parameters used for simulation

Parameter	CZTS-AD[56]	CZTS-340[56]	CZTS-360[56]	CZTS-380[56]
Thickness: μm	3*	3*	3*	3*
Bandgap: eV	1.36*	1.38*	1.55*	1.71*
Electron affinity χ: eV	4.1	4.1	4.1	4.1
Dielectric permittivity	6.5	6.5	6.5	6.5
CB effective density of states: 1/cm^3	8.100×10^{16}	8.100×10^{16}	8.100×10^{16}	8.100×10^{16}
VB effective density of states: 1/cm^3	1.500×10^{19}	1.500×10^{19}	1.500×10^{19}	1.500×10^{19}
Electron mobility: cm^2/Vs	1.851×10^1*	2.466×10^1*	1.467×10^1*	9.786×10^0*
Hole mobility: cm^2/Vs	1.260×10^1	1.260×10^1	1.260×10^1	1.260×10^1
Shallow uniform donor density ND: cm^{-3}	4.831×10^{17}*	1.382×10^{16}*	1.019×10^{16}*	1.635×10^{15}*
Shallow uniform acceptor density NA: cm^{-3}	5.821×10^{17}	1.665×10^{16}	1.228×10^{16}	1.917×10^{15}

*experimental values.

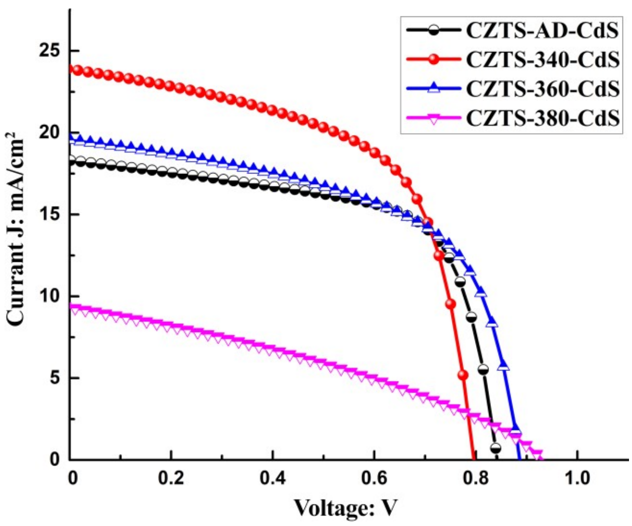

Figure 13. Current plotted against voltage provide from simulation for all CZTS thin films when CdS was used as buffer layer

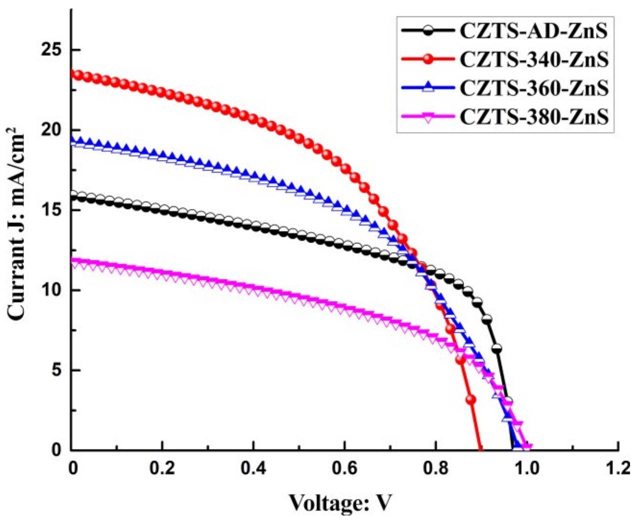

Figure 14. Current plotted against voltage provide from simulation for all CZTS thin films when ZnS was used as buffer layer

with increasing annealing temperature, probably due to the mobility of the sample. It is noteworthy that J_{sc} shows a similar trend in mobility with respect to annealing temperature. Efficient carrier generation for device output depends on timely contact arrival to avoid recombination, which requires long relaxation times and increased mobility.[47] In contrast, the unannealed sample shows J_{sc} values of 19.28 mA cm^{-2} for CdS and 15.93 mA cm^{-2} for ZnS.

Table 5. Scaps-1D results 'efficiency, short-circuit current density, open-circuit voltage, and fill factor' of all CZTS thin film using two different buffer layers

	Buffer layer	CZTS-AD	CZTS-340	CZTS-360	CZTS-380
η (%)	CdS	10.01	11.40	9.99	2.99
	ZnS	8.91	10.55	9.27	5.67
J_{sc} (mA/cm^{-2})	CdS	19.28	23.88	19.55	9.34
	ZnS	15.93	25.26	19.26	11.81
V_{oc} (V)	CdS	0.80	0.79	0.88	0.93
	ZnS	0.97	0.84	0.98	1.00
FF (%)	CdS	64.51	59.88	57.57	34.35
	ZnS	57.56	49.49	49.03	47.92

The CZTS-AD configuration with CdS and ZnS as buffer layers exhibited the highest fill factor (64.51% for CdS and 57.56% for ZnS), which decreased with increasing CZTS annealing temperature. In contrast, the open-circuit voltage of the CZTS thin film increases with annealing temperature, with the lowest V_{oc} observed for CZTS-340 (0.79 V for CdS and 0.84 V for ZnS). In particular, solar cells with ZnS as a buffer layer showed higher V_{oc} values compared to those with CdS. Efficiency is an important parameter for determining the performance of solar cells. The simulation results of the efficiency of the solar cell with CdS and ZnS as the buffer layers are shown in Figure 15. The efficiency of solar cells with CdS or ZnS decreased with increasing annealing temperature. The solar cell with CZTS-AD as the absorbing layer achieved an average efficiency of η_{CdS} = 10.01% and η_{ZnS} = 8.91%. The efficiency values across all samples ranged from 2.99% to 11.40%. The solar cell with CZTS-340 showed the highest efficiency at 11.40% for CdS and 10.55% for ZnS. The solar cell with the CdS buffer layer showed the best performance, compared to that with the ZnS buffer layer. However, solar cells with a ZnS buffer layer (Mo/CZTS/ZnS/ZnO:I) offer numerous advantages. They are crafted from non-toxic, eco-friendly, and abundant materials, resulting in a cost-effective material with an efficiency of 10.55% for the CZTS-340, even without sulfurization. The maximum efficiency values for CdS or ZnS with CZTS-340 as the absorbent layer are within the range of numerous studies.[48,49] However, the experimental results for solar cells produced by spin coating are still behind the simulated ones.[27,50] This discrepancy can cause several problems in solar cell assembly due to interface problems between layers and the appearance of secondary phases in CZTS thin films. The deposition of CZTS on Mo produces MoS_2 with n-type conductivity, which affects the fill factor (FF) and increases the series resistance, which consequently reduces the open-circuit voltage (V_{oc}).[43] The secondary phases of the CZTS layer, such as SnS and ZnS,[51] influence the short-circuit current (I_{sc}) of the solar cell, while V_{oc} is limited by Cu_2SnS_3.[52,53]

Figure 16 shows the efficiency of CZTS/ZnS/ZnO based on the composition map determined by the Zn/Sn and Cu/Zn + Sn ratios. The simulated results show that the most efficient performance of 10.55% is achieved with CZTS thin films annealed at 340°C in the low Cu and high Zn region. This result is in good agreement with the experimental one. In a study by Katagiri *et al.*,[54] the influence of composition on the efficiency of CZTS solar cells was investigated by adjusting the molar ratios of Cu/Sn + Zn and Zn/Sn. They found that the highest efficiency was achieved in the Cu-poor and Zn-rich region, near the ratios Cu/Zn + Sn = 0.9 and Zn/Sn = 1.25. The CZTS samples annealed at 340°C and 360°C came to this composition with ratios of Cu/Zn + Sn = 0.67 and Zn/Sn = 1.01 as well as Cu/Zn + Sn = 0.92 and Zn/Sn = 1.14 very close, respectively, which leads to efficiencies of 10.55% and 9.27% when ZnS is used as a buffer layer. Deviations from this

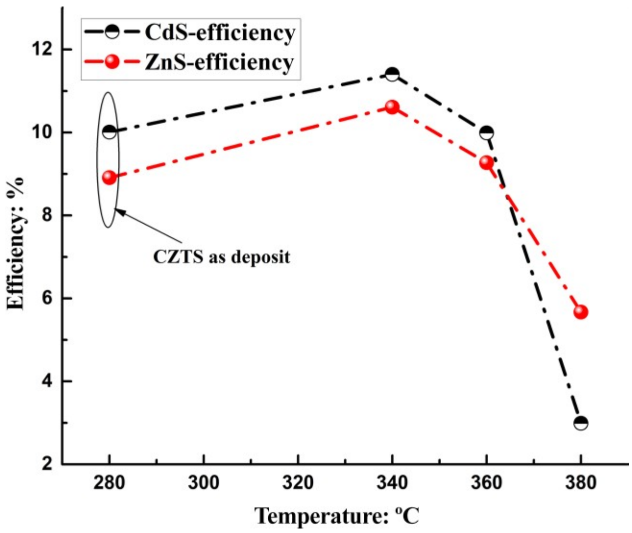

Figure 15. Solar cell efficiency variation with temperatures for two different buffer layers

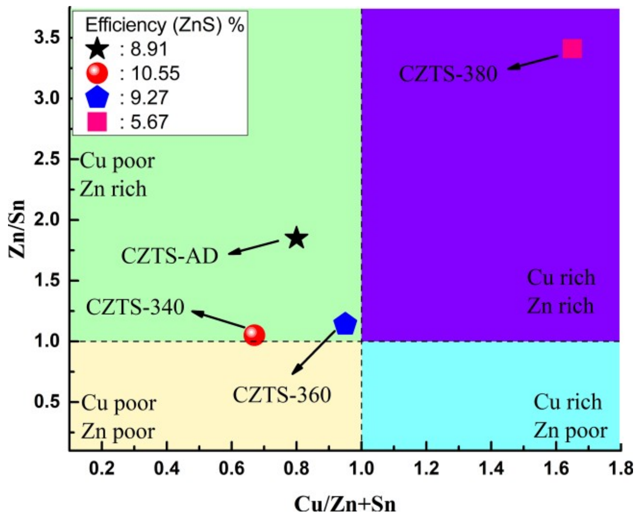

Figure 16. ZnS efficiency plotted against map composition of CZTS annealed at different temperature

optimal configuration resulted in lower efficiency, as shown by the example of CZTS-380, which had the lowest efficiency with Cu/Zn + Sn = 1.65 and Zn/Sn = 3.41 in its composition.

6. Conclusion

We successfully deposited CZTS films at different temperatures on a glass substrate using a low-cost sol-gel spin-coating technique. It is clearly observed that changing the annealing temperature has a significant effect on the physical properties of CZTS thin films. XRD revealed a kesterite structure for all CZTS thin films with a preferential orientation along the (002) plane, and an increase in the crystalline size with annealing temperature was observed. The existence of the CZTS phase observed by XRD was also confirmed by the Raman spectra which showed a peak corresponding to the A1 vibration. The absorption coefficient was estimated from the U-V results and was found at the range of 10^4 cm^{-1} in the visible region. The optical bandgap increases from 1.38 to 1.71 eV with the increase annealing temperature due to the changing at the elemental composition. The electrical properties revealed that the CZTS thin films have P-type conductivity, and minimum resistivity was observed for the CZTS-360 of 1.60×10^{-2} Ω cm. In addition, the *I–V* characterization of CZTS deposited on the ITO substrate confirms the formation of a PN junction by indicating rectifying and non-ohmic behavior. Indeed, the data of all CZTS thin films were injected into the simulation program to study the possibility of using these samples as absorbent layers in solar cells (Mo/CZTS/(CdS or ZnS)/ZnO:I). Furthermore, we investigated the performance of non-toxic and abundant solar cells with ZnS as a buffer layer by comparing it with a solar cell where CdS was used as the buffer layer. A promising efficiency was observed for the solar cell (Mo/CZTS/ZnS/ZnO:I) which varied with the annealing temperature of CZTS from 5.67% to 10.55%.

Funding

The authors declare that no funds, grants, or other support were received during the preparation of this manuscript.

Author contributions

E. El Mahboub: Writing – carried out the experiment (Thesis). S. Zakria: Original draft preparation – analysis and interpretation of data (Thesis). M. Mansori: Visualization, investigation. A. El Hichou: Conception and design of study – reviewing and editing.

Declaration of competing interest

The authors declare that they have no known competing financial interests or personal relationships that could have appeared to influence the work reported in this paper.

REFERENCES

1. Olgar MA, Erkan S and Zan R (2023) Dependence of CZTS thin film properties and photovoltaic performance on heating rate and sulfurization time. *Journal of Alloys and Compounds* **963**: 171283, 10.1016/j.jallcom.2023.171283.
2. Zakaria S, El Mahboub E and EL Hichou A (2023) Physical properties of the low-cost CZTS absorber layer deposited by spin-coating: effect of the copper concentration associated with SCAPS-1D simulation. *RSC Advances* **13(39)**: 27106–27115, 10.1039/D3RA03996J.
3. Erkan S, Yagmyrov A, Altuntepe A, Zan R and Olgar MA (2022) Integration of single layer graphene into CZTS thin film solar cells. *Journal of Alloys and Compounds* **920**: 166041, 10.1016/j.jallcom.2022.166041.
4. Chauhan P, Agarwal S, Srivastava V *et al.* (2023) Kesterite CZTS based thin film solar cell: Generation, recombination, and performance analysis. *Journal of Physics and Chemistry of Solids* **183**: 111631, 10.1016/j.jpcs.2023.111631.
5. Woo K, Kim Y, Yang W *et al.* (2013) Band-gap-graded $Cu_2ZnSn(S_{1-x},Se_x)_4$ solar cells fabricated by an ethanol-based, particulate precursor ink route. *Scientific Reports* **3**: 3069, 10.1038/srep03069.
6. Wang W, Winkler MT, Gunawan O *et al.* (2014) Device characteristics of CZTSSe thin-film solar cells with 12.6% efficiency. *Advanced Energy Materials* **4(7)**: 1–5, 10.1002/aenm.201301465.
7. Shimamune Y, Jimbo K, Nishida G *et al.* (2017) Cu2ZnSnS4 formation by co-evaporation and subsequent annealing in S-flux using molecular beam epitaxy system. *Thin Solid Films* **638**: 312–317, 10.1016/j.tsf.2017.08.002.
8. Yang J, Xu J, Miao D and Jiang S (2021) Compositional, structural, morphological, and optical characterization of magnetron sputtered CZTS thin films from various argon flow rate. *Physica B: Condensed Matter* **623**: 413375, 10.1016/j.physb.2021.413375.
9. Gansukh M, López Mariño S, Espindola Rodriguez M *et al.* (2020) Oxide route for production of Cu2ZnSnS4 solar cells by pulsed laser deposition. *Solar Energy Materials and Solar Cells* **215**: 110605, 10.1016/j.solmat.2020.110605.
10. Dridi S, Bitri N, Aubry E, Mahjoubi S and Briois P (2024) Comparative study of Cu2XSnS4 (X = Ni, Co, Mn or Fe) films synthesized by spray pyrolysis under air atmosphere, as suitable absorber layers for photovoltaic applications. *Journal of Alloys and Compounds* **976**: 172976, 10.1016/j.jallcom.2023.172976.
11. Demir KÇ (2021) The investigation of the corrosion behavior of CZTS thin films prepared via electrodeposition. *Materials Science in Semiconductor Processing* **123**: 105553, 10.1016/j.mssp.2020.105553.
12. Özdal T and Kavak H (2021) Single step amperometric growth of CZTS thin film: deposition current and stoichiometry relationship. *Ceramics International* **47(17)**: 24841–24851, 10.1016/j.ceramint.2021.05.210.
13. Özdal T and Kavak H (2017) Comprehensive analysis of spin coated copper zinc tin sulfide thin film absorbers. *Journal of Alloys and Compounds* **725**: 644–651, 10.1016/j.jallcom.2017.07.209.
14. Boudaira R, Meglali O, Bouraiou A *et al.* (2020) Optimization of sulphurization temperature for the production of single-phase CZTS kesterite layers synthesized by electrodeposition. *Surface Engineering* **36(9)**: 1000–1011, 10.1080/02670844.2020.1758013.
15. Prabeesh P, Saritha P, Selvam IP and Potty SN (2017) Fabrication of CZTS thin films by dip coating technique for solar cell applications. *Materials Research Bulletin* **86**: 295–301, 10.1016/j.materresbull.2016.10.033.
16. Xu J, Yang J, Jiang S and Shang S (2020) Effects of element ratio on robustness of CZTS films: variations in sulfurization temperature. *Ceramics International* **46(16)**: 25927–25934, 10.1016/j.ceramint.2020.07.079.
17. Yu X, Ren A, Wang F *et al.* (2014) Synthesis and characterization of CZTS thin films by sol-gel method without sulfurization. *International Journal of Photoenergy* **2014**: 1–6, 10.1155/2014/861249.
18. Khottummee N, Samphao T, Samapisut S, Aung S and Seetawan T (2018) Synthesis and optical properties of porous CZTS films deposited by dip coating technique. *International Journal of Recent Engineering Research and Development* **3(1)**: 18–24.

19. Maeda K, Tanaka K, Nakano Y and Uchiki H (2011) Annealing temperature dependence of properties of Cu_2ZnSnS_4 thin films prepared by sol–gel sulfurization method. *Japanese Journal of Applied Physics* **50(5S2)**: 05FB08, 10.1143/JJAP.50.05FB08.
20. Park H, Hwang YH and Bae B-S (2013) Sol–gel processed Cu2ZnSnS4 thin films for a photovoltaic absorber layer without sulfurization. *Journal of Sol-Gel Science and Technology* **65(1)**: 23–27, 10.1007/s10971-012-2703-0.
21. Benachour MC, Bensaha R and Moreno R (2019) Annealing duration influence on dip-coated CZTS thin films properties obtained by sol-gel method. *Optik (Stuttg)* **187**: 1–8, 10.1016/j.ijleo.2019.05.015.
22. Burgelman M, Verschraegen J, Degrave S and Nollet P (2004) Modeling thin-film PV devices. *Progress in Photovoltaics: Research and Applications* **12(2–3)**: 143–153, 10.1002/pip.524.
23. Sherrer P (1918) Determination of the size and internal structure of colloidal particles using X rays. *Nachrichten von der Gesellschaft der Wissenschaften zu Göttingen* **394**: 98–100.
24. Revathi N, Prathap P, Miles RW and Ramakrishna Reddy KT (2010) Annealing effect on the physical properties of evaporated In 2S3 films. *Solar Energy Materials and Solar Cells* **94(9)**: 1487–1491, 10.1016/j.solmat.2010.02.044.
25. Özdal T and Kavak H (2018) Determination of crystallization threshold temperature for sol-gel spin coated Cu2ZnSnS4 thin films. *Ceramics International* **44(15)**: 18928–18934, 10.1016/j.ceramint.2018.07.129.
26. Hong S (2024) Investigation of gradient band gap in Cu2ZnSnS4 thin films with residual strain. *Current Applied Physics* **58**: 65–73, 10.1016/j.cap.2023.12.005.
27. Park SN, Sung SJ, Son DH *et al.* (2014) Solution-processed Cu2ZnSnS4 absorbers prepared by appropriate inclusion and removal of thiourea for thin film solar cells. *RSC Advances* **4(18)**: 9118–9125, 10.1039/c3ra45441j.
28. Chen S, Wang LW, Walsh A, Gong XG and Wei SH (2012) Abundance of CuZn+ SnZn and 2CuZn +Sn Zn defect clusters in kesterite solar cells. *Applied Physics Letters* **101(22)**: 1–5, 10.1063/1.4768215.
29. Jeganath K, George SD, Murari MS and Raviprakash Y (2021) Effect of sulfurization temperature on Cu-Zn disorder for non-stoichiometric spray pyrolyzed Cu2ZnSnS4 thin films. *Materials Letters* **300**: 130168, 10.1016/j.matlet.2021.130168.
30. Khelfane A, Ziane MI, Tablaoui M *et al.* (2023) Composition dependence of the optical band gap and the secondary phases via zinc content in CZTS material. *Inorganic Chemistry Communications* **151**: 110639, 10.1016/j.inoche.2023.110639.
31. Elmahboub E, Hichou AE and Mansori M (2022) The nontoxic and the low-cost solution-processed CZTS absorber layer for solar photovoltaic application: effect of solvent on physical properties. *Physica Status Solidi* **219(10)**: 2100882.
32. Seboui Z, Cuminal Y and Kamoun-Turki N (2013) Physical properties of Cu_2ZnSnS_4 thin films deposited by spray pyrolysis technique. *Journal of Renewable and Sustainable Energy* **5(2)**: 023113, 10.1063/1.4795399.
33. Sánchez TG, Mathew X and Mathews NR (2016) Obtaining phase-pure CZTS thin films by annealing vacuum evaporated CuS/SnS/ZnS stack. *Journal of Crystal Growth* **445**: 15–23, 10.1016/j.jcrysgro.2016.03.039.
34. Feng J, Huang X, Chen W *et al.* (2016) Fabrication and characterization of Cu2ZnSnS4 thin films for photovoltaic application by low-cost single target sputtering process. *Vacuum* **126**: 84–90, 10.1016/j.vacuum.2016.01.023.
35. Larramona G, Bourdais S, Jacob A *et al.* (2014) 8.6% Efficient CZTSSe solar cells sprayed from water-ethanol CZTS colloidal solutions. *Journal of Physical Chemistry Letters* **5(21)**: 3763–3767, 10.1021/jz501864a.
36. Seol J, Lee S, Lee J, Nam H and Kim K (2003) Electrical and optical properties of CuZnSnS thin films prepared by rf magnetron sputtering process. *Solar Energy Materials and Solar Cells* **75(1–2)**: 155–162, 10.1016/S0927-0248(02)00127-7.
37. Chen S, Wang L-W, Walsh A, Gong XG and Wei S-H (2012) Abundance of Cu Zn + Sn Zn and 2Cu Zn + Sn Zn defect clusters in kesterite solar cells. *Applied Physics Letters* **101(22)**: 223901, 10.1063/1.4768215.
38. Ziti A, Hartiti B, Labrim H *et al.* (2019) Study of kesterite CZTS thin films deposited by spin coating technique for photovoltaic applications. *Superlattices Microstruct* **127**: 191–200, 10.1016/j.spmi.2017.11.023.
39. Patel M, Mukhopadhyay I and Ray A (2012) Structural, optical and electrical properties of spray-deposited CZTS thin films under a non-equilibrium growth condition. *Journal of Physics D: Applied Physics* **45(44)**: 445103, 10.1088/0022-3727/45/44/445103.
40. Diwate K, Mohite K, Shinde M *et al.* (2017) Synthesis and characterization of chemical spray pyrolysed CZTS thin films for solar cell applications. *Energy Procedia* **110**: 180–187, 10.1016/j.egypro.2017.03.125.
41. Vikas LS, Sanal KC, Jayaraj MK, Antony A and Puigdollers J (2014) Vertically aligned ZnO nanorod array/CuO heterojunction for UV detector application. *Physica Status Solidi (A)* **211(11)**: 2493–2498, 10.1002/pssa.201431221.
42. Covei M, Perniu D, Bogatu C and Duta A (2019) CZTS-TiO2 thin film heterostructures for advanced photocatalytic wastewater treatment. *Catalysis Today* **321–322**: 172–177, 10.1016/j.cattod.2017.12.003.
43. Gunavathy KV, Tamilarasan K, Rangasami C and Arulanantham AMS (2020) Investigations on copper zinc tin sulfide thin films grown through nebulizer assisted spray pyrolysis technique. *International Journal of Energy Research* **44(9)**: 7371–7385, 10.1002/er.5451.
44. Khemiri N, Aousgi F and Kanzari M (2017) Tunable optical and structural properties of Zn(S,O) thin films as Cd-free buffer layer in solar cells. *Materials Letters* **199**: 1–4, 10.1016/j.matlet.2017.04.037.
45. Gour KS, Parmar R, Kumar R and Singh VN (2020) Cd-Free Zn(O,S) as alternative buffer layer for chalcogenide and kesterite based thin films solar cells: a review. *Journal of Nanoscience and Nanotechnology* **20(6)**: 3622–3635, 10.1166/jnn.2020.17537.
46. Abdolahzadeh Ziabari A, Mohabbati Zindanlou N, Hassanzadeh J, Golshahi S and Bagheri Khatibani A (2020) Fabrication and study of single-phase high-hole-mobility CZTS thin films for PV solar cell applications: influence of stabilizer and thickness. *Journal of Alloys and Compounds* **842**: 155741, 10.1016/j.jallcom.2020.155741.
47. Tousif MN, Mohamma S, Ferdous AA and Hoque MA (2018) Investigation of different materials as buffer layer in CZTS solar cells using SCAPS. *Journal of Clean Energy Technologies* **6(4)**: 293–296, 10.18178/jocet.2018.6.4.477.
48. Jhuma FA, Shaily MZ and Rashid MJ (2019) Towards high-efficiency CZTS solar cell through buffer layer optimization. *Materials for Renewable and Sustainable Energy* **8(1)**: 1–7, 10.1007/s40243-019-0144-1.
49. Agawane GL, Kamble AS, Vanalakar SA *et al.* (2015) Fabrication of 3.01% power conversion efficient high-quality CZTS thin film solar cells by a green and simple sol-gel technique. *Materials Letters* **158**: 58–61, 10.1016/j.matlet.2015.05.036.
50. Ferdaous MT, Shahahmadi SA, Chelvanathan P *et al.* (2019) Elucidating the role of interfacial MoS_2 layer in Cu_2ZnSnS_4 thin film solar cells by numerical analysis. *Solar Energy* **178**: 162–172, 10.1016/j.solener.2018.11.055.
51. Wang K, Gunawan O, Todorov T *et al.* (2010) Thermally evaporated Cu_2ZnSnS_4 solar cells. *Applied Physics Letters* **97(14)**: 8–11, 10.1063/1.3499284.
52. Wang W, Chen G, Cai H *et al.* (2018) The effects of SnS_2 secondary phases on Cu_2ZnSnS_4 solar cells: a promising mechanical

exfoliation method for its removal. *Journal of Materials Chemistry A* **6(7)**: 2995–3004, 10.1039/C7TA08242H.

53. Yan C, Huang J, Sun K *et al.* (2018) Cu2ZnSnS4 solar cells with over 10% power conversion efficiency enabled by heterojunction heat treatment. *Nature Energy* **3(9)**: 764–772, 10.1038/s41560-018-0206-0.
54. Katagiri H, Jimbo K, Tahara M, Araki H and Oishi K (2009) The influence of the composition ratio on CZTS-based thin film solar cells. *MRS Proceedings* **1165**: 1165-M04-01, 10.1557/PROC-1165-M04-01.
55. Jhuma FA and Rashid MJ (2020) Simulation study to find suitable dopants of CdS buffer layer for CZTS solar cell. *Journal of Theoretical and Applied Physics* **14(1)**: 75–84, 10.1007/s40094-019-00363-3.
56. Sharbati S, Norouzzadeh E and Mohammadi S (2018) A simulation study to improve the efficiency of $ZnO_{1-x}S_x/Cu_2ZnSn\ (S_y, Se_{1-y})_4$ solar cells by composition-ratio control. *Optical Materials* **78**: 259–265, 10.1016/j.optmat.2018.02.032.